Second International Symposium on Marine Propulsors
smp'11, Hamburg, Germany, June 2011
Workshop: Propeller performance

Prediction of Non-Cavitating and Cavitating Performance of a SVA Potsdam Propeller

Da-Qing Li

SSPA Sweden AB, Gothenburg, Sweden

ABSTRACT

The paper presents numerical results of open water characteristics (Case 2.1), flow field (Case 2.2) and cavitation behaviour (Case 2.3) of a CP propeller provided by SVA Potsdam for the SMP'11 Workshop on Cavitation and Propeller Performance. Steady incompressible RANS method with a SST k-ω turbulence model available in FLUENT 12.1 is employed. In the case of cavitation flows, the homogeneous multi-phase mixture RANS method and Schnerr-Sauer's cavitation model are used. A wall-resolved mesh, ensuring a y+=1, is used for all three cases. Flow analysis for the non-cavitating condition reveals that there is a tip vortex developed at blade tip and the tip vortex survives a short distance downstream the blade tip. Steady sheet cavity on suction side, tip vortex, root and hub cavitation are noted in one off-design condition. At the operation point, extensive root cavitation on both pressure and suction side, and a rather weak tip vortex cavity are observed. In another off-design condition, a narrow pressure side sheet cavity with minor root cavitation is found.

Keywords

Propeller, cavitation, cavitation model, multi-phase, turbulence.

1 INTRODUCTION

A CP propeller with extensive measurement data was provided by SVA Potsdam with well-defined cases and conditions for the SMP'11 Workshop on Cavitation and Propeller Performance. The experiment datasets cover the open water characteristics, LDV measurements of velocity field (non-cavitating) and cavitation tests. The workshop for this propeller is organized in a "blind test" format that none of the participants knows the experiment results prior to the workshop. SSPA Sweden AB participates all the three validation cases.

2 NUMERICAL METHODS

Multi-phase model

The multi-phase mixture model in FLUENT12.1 assumes that the working medium is a single fluid with a homogeneous mixture of two phases (liquid and vapor). Denoting the density of the mixture by ρ_m, the continuity equation for the mixture flow becomes:

$$\frac{\partial}{\partial t}(\rho_m) + \nabla \cdot (\rho_m \vec{v}_m) = 0 \tag{1}$$

The momentum equation for the mixture reads:

$$\frac{\partial}{\partial t}(\rho_m \vec{v}_m) + \nabla \cdot (\rho_m \vec{v}_m \vec{v}_m) = -\nabla p + \nabla \cdot \left[\mu_m \left(\nabla \vec{v}_m + \nabla \vec{v}_m \right) \right] + \rho_m \vec{g} + \vec{F} \tag{2}$$

The density relation of each phase in a mixture-flow cell is described by means of a scalar volume fraction as:

$$\rho_m = \alpha_v \rho_v + (1-\alpha_v)\rho_l \tag{3}$$

where α_v is the volume fraction of vapor. To account for the mass transfer between phases a cavitation model and close the equation system, an additional transport equation is needed for α_v as shown below. Note for the wetted flow cases, ρ_m is replaced by ρ_l in Eq. (1)-(2) to retain the conventional forms of RANS eqs.

Cavitation model

The cavitation model used for 2D foil is developed by Schnerr and Sauer (2001). It solves for the vapor volume fraction with the following transport equation:

$$\frac{\partial}{\partial t}(\alpha_v \rho_v) + \nabla \cdot (\alpha_v \rho_v \vec{v}_m) = R_e - R_c \tag{4}$$

The source terms R_e and R_c were derived from the bubble dynamics equation of Rayleigh-Plesset and account for the mass transfer between the vapor and liquid phases in cavitation. They have the following form:

$$R_e = \frac{\rho_v \rho_l}{\rho_m} \alpha (1-\alpha) \frac{3}{\Re_B} \sqrt{\frac{2}{3} \frac{(p_v - p)}{\rho_l}} \tag{5}$$

when $p_v > p$, and

$$R_c = \frac{\rho_v \rho_l}{\rho_m} \alpha (1-\alpha) \frac{3}{\Re_B} \sqrt{\frac{2}{3} \frac{(p - p_v)}{\rho_l}} \tag{6}$$

when $p_v < p$. The bubble radius R_B can be determined by:

$$\Re_B = \left(\frac{\alpha}{1-\alpha} \frac{3}{4\pi} \frac{1}{n_0} \right)^{1/3} \tag{7}$$

where n_0 is the bubble number density. A default value $n_0 = 10^{13}$ is used here.

The second order QUICK scheme is used for convection terms for all cases. A fully coupled solver is used to solve pressure and momentum equations. More detail of methodology can be found in (Li et al. 2009).

3 LOADINGS AND GRIDS

The loading conditions for the three cases are summarized in the table below. Further details of the case definition can be found in the workshop proceedings.

Table 1 Load conditions

	n [1/s]	V [m/s]	K_T[-] Thrust identity	σ_n[-]
Case 2.1	15	2.25~5.25	Open water performance	-
Case 2.2	23	-	0.250	-
Case 2.3.1	24.987	-	0.387	2.204
Case 2.3.2	24.986	-	0.245	1.424
Case 2.3.3	25.014	-	0.167	2.000

For propeller operating in a uniform inflow, periodic boundary conditions can be utilized in the circumferential direction. A blade passage with 72° periodicity in the circumferential direction constitutes the computational domain. Hexahedral meshes are generated in the domain using ANSYS ICEMCFD 12.1, see Figure 1~2. The inlet plane is located at 2D (D=propeller diameter) upstream and the outlet plane at 4D downstream the propeller center. The outer boundary in the radial direction is placed at radius=3D for the open water calculations. For Case 2.2 and Case 2.3, the outer boundary radius is set to 1.356D, giving an equivalent cross section area to that of cavitation tunnel in the cavitation test.

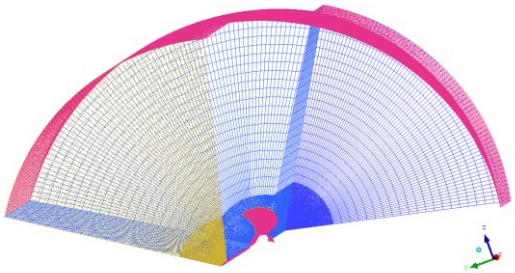

Figure 1 Meshes on computational domain surface

Figure 2 Surface mesh on the blade

The boundary conditions (BC) are as follows:
Inlet BC: constant velocity (based on load condition). Turbulence intensity and turbulent viscosity ratio are set to 5 and 10 respectively.
Blade/hub: no-slip wall.
Outlet: pressure outlet (based on cavitation number).
Outer boundary: symmetry BC.

Note that there is a fillet between the blade root and the hub original propeller geometry, to avoid badly skewed hexa cells this fillet is not included. It means that there is a minor difference between the original geometry and the one used in the present work.

4 RESULTS

4.1 Open water characteristics (Case 2.1)

For open water performance calculations, the propeller is arranged in a pulling configuration, the same as in the open water tests. The mesh consists of 996000 hexahedral cells and the grid lines perpendicular to wall are refined substantially to obtain a y+=1 for the first grid cell layer. The rate of revolution is kept constant whereas the inflow speed is varied to achieve different advance ratios. The open water characteristics curve is given in Figure 3.

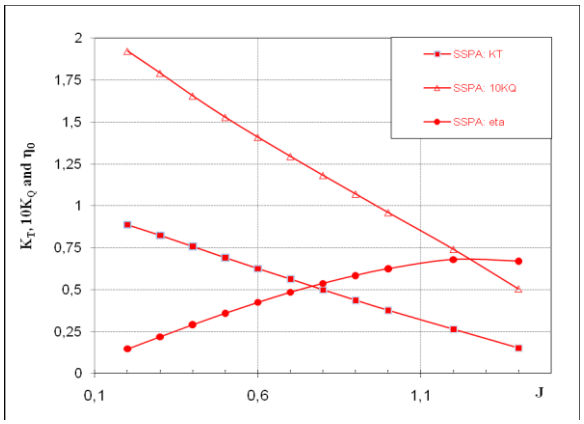

Figure 3 open water characteristics curve

4.2 Flow field (Case 2.2)

The same propeller blade geometry as in Case 2.1 is used for Case 2.2 and 2.3. However, the propeller is now placed in a pushing mode operating inside a circular cavitation tunnel. The mesh for Case 2.2 and 2.3 consists of 1496000 hexahedral cells. After simulation, a coordinate transformation is necessary to comply with the coordinate system defined by the workshop.

The calculation was carried out according to the thrust identity method. With the rate of revolution n=23 1/s fixed and K_T=0.25 as target thrust, the inlet velocity is progressively decreased from 7.2 m/s to a final value of 7.15 m/s (corresponding to a J=1.243). Figure 4 shows the contour plot of pressure coefficient (Cp) distribution on the pressure (left) and suction side (right). The minimum Cp is found to be -4.952, located at the tip vortex core

slightly downstream the blade tip. The Cp is non-dimensionalised by $\frac{1}{2}\rho(nD)^2$.

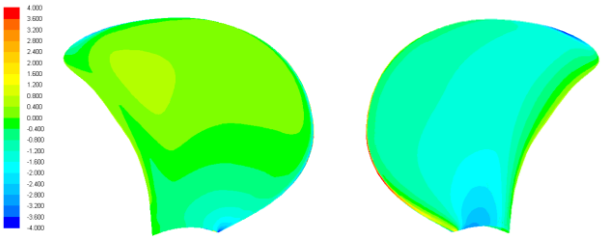

Figure 4 Cp on pressure side (left) and suction side (left)

The axial velocity at a plane with angular position ϕ=-20° is shown in Figure 5. The tip vortex flow structure is clearly visible immediately downstream the blade tip. However, the intensity of tip vortex decreases rapidly after one blade revolution and almost vanishes completely from the third revolution and thereafter. This is a clear indication of a too coarse grid resolution downstream the blade.

Vortical flow can be visualized by other measures. Vorticity, defined as $|\omega|=|\nabla\times\mathbf{u}|$, can be one measure. An iso-surface of vorticity of a magnitude $|\omega|$=460 is shown in Figure 6. An iso-surface of the second eigenvalue (λ_2) of the squared-sum of the symmetric and antisymmetric tensor of $\nabla\mathbf{u}$ is shown in Figure 7. For its definition, see Jeong and Hussain (1995). These plots also indicate the existence of tip vortex downstream the blade tip, as well as its rapid dissipation further downstream.

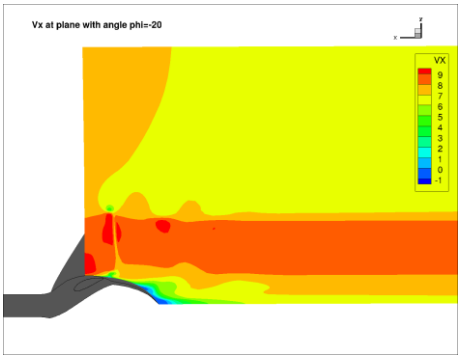

Figure 5 Axial velocity at angular plane ϕ=-20°

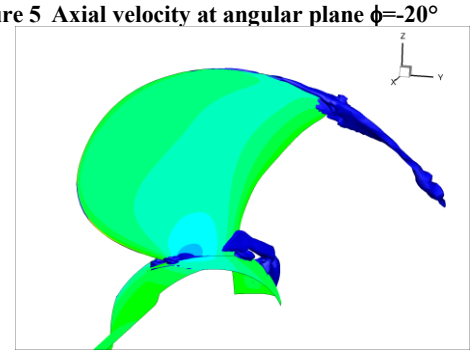

Figure 6 Iso-surface of |vorticity| =460

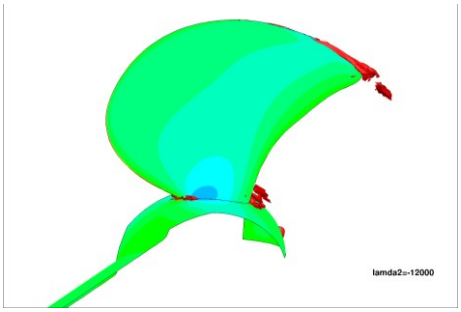

Figure 7 Iso-surface of λ_2=-12000

4.3 Cavitation behavior (Case 2.3)

The calculations for all the cavitation cases are based on the thrust identity method, following the workshop recommended procedure. Namely, start with wetted flow computation with the fixed rate of revolution and the given K_T as target thrust, the inlet velocity is progressively adjusted so that the computed K_T approaches the target one. Then the tunnel pressure is lowered to match the given cavitation number and cavitation calculation is performed with a so-determined inlet velocity.

Case 2.3.1

A stable and narrow sheet cavity is observed on the suction side of the blade in this case. At outer radii, the sheet cavity merges into a tip vortex cavity. In addition, root cavitation is found at the mid-chord of the blade root. The cavitation patterns are illustrated by an iso-surface of α_v=0.5 shown in Figure 8. Figure 9 is a side view of the same plot, where hub vortex cavitation is visible. The shape of cavity is not very much influenced by the selected iso-value of α_v, meaning that the cavity interface is thin. The predicted K_T is about 0.388 with a σ_n=2.024.

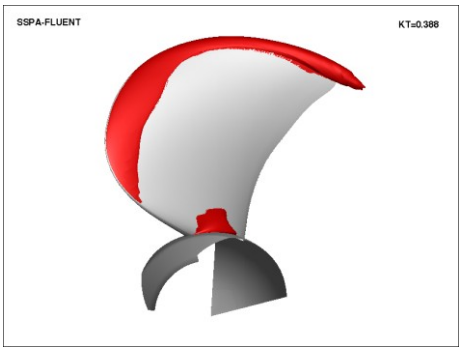

Figure 8 iso-surface of α_v =0.50 case 2.3.1

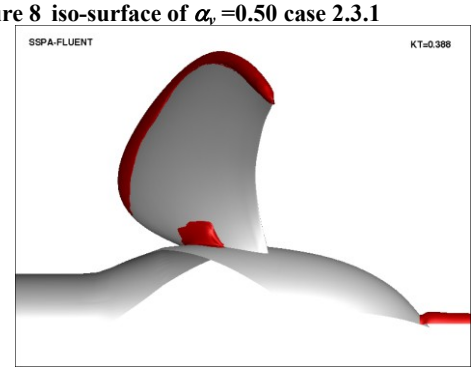

Figure 9 iso-surface of α_v =0.50 case 2.3.1, side view

The pressure coefficients cp at three radial sections are compared for the non-cavitating and cavitating flows in Figure 10. Note here the cp is non-dimensionalised by the resultant inflow velocity according to the workshop definition.

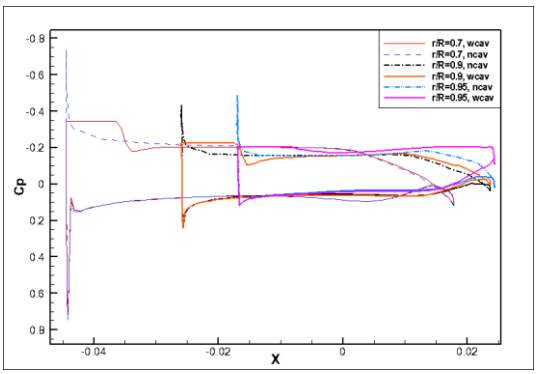

Figure 10 Cp comparison for non-cav. and cavitating flows

Case 2.3.2

For Case 2.3.2, a weak tip vortex cavity and substantial mid-chord root cavitation are observed on the suction side, see Figure 11. Furthermore, on the pressure side there is a narrow sheet cavity along the leading edge and some root cavitation at mid-chord root. The cavitation pattern on the pressure side is depicted in Figure 12. No hub cavitation is present. The predicted K_T is about 0.205 with a σ_n=1.424.

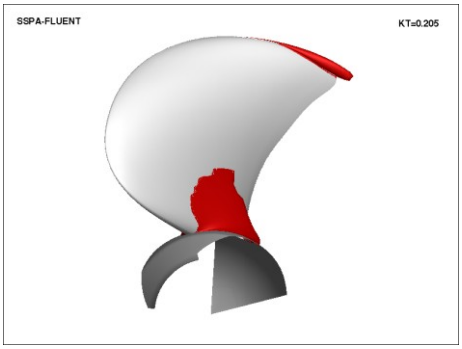

Figure 11 iso-surface of α_v =0.50 case 2.3.2, suction side

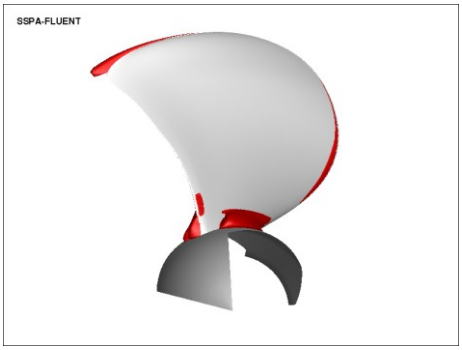

Figure 12 iso-surface of α_v =0.50 case 2.3.2, pressure side

Case 2.3.3

At this loading and cavitation number, a narrow stable sheet cavity is observed on the pressure side of the blade, together with some root cavitation, see Figure 13 and Figure 14. No hub cavitation is present. The predicted K_T is about 0.144 with a σ_n=2.000.

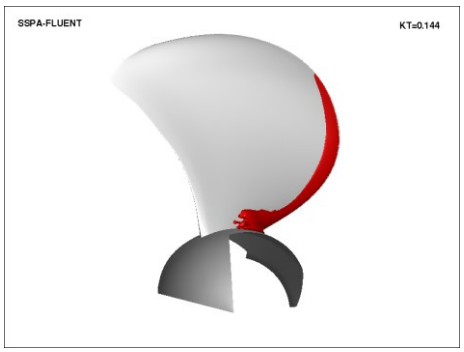

Figure 13 iso-surface of α_v =0.50 case 2.3.3

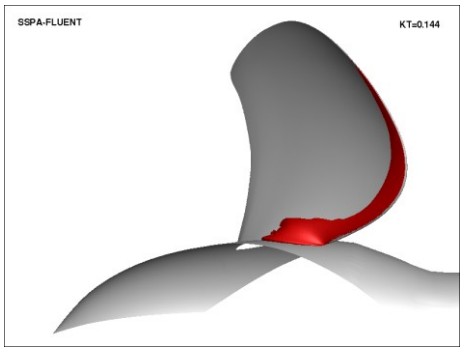

Figure 14 iso-surface of α_v =0.50 case 2.3.3, side view

6 CLOSING REMARKS

For the open water performance prediction, case 2.1, a mesh of 996000 cells is used. For case 2.2 and 2.3, a mesh of 1496000 cells is used. While the flow around blade seems to be well resolved the present mesh resolution behind propeller blade is not fine enough to capture the tip vortex flows downstream the blade tip. Alternatively, a local mesh adaptation along the tip vortex trace would have improved the resolution of tip vortex flow.

REFERENCES

Schnerr, G. H. and Sauer J., (2001), 'Physical and Numerical Modeling of Unsteady Cavitation Dynamics', In Fourth International Conference on Multiphase Flow, New Orleans, USA.

Jeong, J.H. and Hussain, F. (1995) 'On the identification of a vortex', Journal of Fluid Mechanics, Vol. 285.

Li, D.-Q., Grekula, M. and Lindell, P. (2009), 'A modified SST k-□ Turbulence Model to Predict the Steady and Unsteady Sheet Cavitation on 2D and 3D Hydrofoils', The 7th International Symposium on Cavitation (CAV2009), Michigan, USA.